Results in Physics 45 (2023) 106258

Contents lists available at ScienceDirect

Results in Physics

journal homepage: www.elsevier.com/locate/rinp

An ultrahigh-resolution spectrometer using parallel double gratings

Jun Chen [a,b,c], Xiaotian Li [a,b,c,*], Qihang Chu [a,b,c], Jiri Galantu [a,c], Yuqi Sun [a,b,c], Bo Zhang [a,c], Ba Yanheshig [a,c]

[a] Changchun Institute of Optics, Fine Mechanics and Physics, Chinese Academy of Sciences, Changchun Jilin 130033, China
[b] University of Chinese Academy of Sciences, Beijing 100049, China
[c] National Engineering Research Center for Diffraction Gratings Manufacturing and Application, Changchun Jilin 130033, China

ARTICLE INFO

Abbreviations:
spectrometer
gratings
ultrahigh resolution
theoretical analysis

ABSTRACT

This paper describes a Parallel-Double-Grating Spectrometer (PDGS) with ultrahigh resolution. Two plane reflection gratings are placed in parallel and staggered to form a dispersive component, through which the light passes multiple times, which greatly improves the dispersion capability of the spectrometer, and therefore the resolution. The diffraction characteristics of the dispersive component and the mathematical model of the PDGS are studied. The results of simulation show that using two reflection gratings with a groove density of 168 gr/mm, combined with spectral splicing technology, the PDGS can achieve a measurement waveband from 450 nm to 610 nm with a resolution better than 30.88 pm. Modifying the structural parameters of the PDGS extends the applicability of the optical path structure to spectral bands from ultraviolet to infrared.

Introduction

Spectrometers can obtain the spectral characteristic information of substances, so they play an important role in analyzing the components and the physical and chemical properties of many substances. Higher spectral resolution means that the spectrometer can acquire finer spectral peaks [1], which in turn improves the spectrometer's ability to distinguish different substances. For example, in the field of astronomy, the high spectral resolution allows Doppler separation of spectral lines in a planet's atmosphere from those in the Earth's, enabling the detection and measurement of secondary and isotopic components in the planet's atmosphere [2–4]. In the field of biomedicine, high-resolution spectrometers are required to identify Brillouin frequency shifts to obtain viscoelastic properties of biological tissues [5,6]. In the field of optical fiber communication, density wavelength-division multiplexing (DWDM) optical communication systems have nano- or sub-nano-spaced channels in the infrared range; a high-resolution spectrometer is required to accurately measure the optical signal-to-noise ratio of the DWDM system [7]. In addition, high-resolution spectroscopy technology [8–12] is widely used in the characterization and evaluation of optical frequency comb sources [13,14], characterizing the narrow linewidth laser source, [15,16] and other research fields.

According to the classification of spectral information acquisition, spectrometers can be divided into three types: dispersive [17], interference [18], and filter [19]. The diffractive optical elements of dispersive spectrometers are usually prisms and gratings [20]. Compared with prisms, grating's dispersion capacity is stronger. In most optical path designs of grating spectrometers, the detected light passes through the grating only once—only one dispersion of the measured light is performed[21]. And grating's resolving power is restricted by the product of the total number of grating lines and the diffraction order used [22]. In this case, the grating usually provides resolving power from 1,000 to 100,000 [23]. For example, the Czerny-Turner spectrometer adopts a reflective off-axis structure which usually provides nanoscale-level or sub nanoscale-level resolution [23,24]. To further improve the spectral resolution of spectrometers, in terms of the classic design method, optical devices with large apertures and long focal lengths are required as well as higher groove densities and larger gratings. Another way to obtain higher resolution is to disperse the signal light multiple times [25–27], possibly by connecting two or three spectrometers in series [28]; the cascaded spectrometer system is not only large and complicated but also expensive.

In this study, we developed a spectrometer design that uses two flat reflection gratings with the same groove density to achieve ultra-high resolution. The proposed spectrometer has a compact structure, of which the main component is the parallel double gratings named PDG. In this system, the light to be measured is diffracted back and forth between two parallel plane reflection gratings to acquire *N*-fold

* Corresponding author.
E-mail address: lixiaotian@ciomp.ac.cn (X. Li).

https://doi.org/10.1016/j.rinp.2023.106258
Received 9 December 2022; Received in revised form 27 January 2023; Accepted 1 February 2023
Available online 3 February 2023

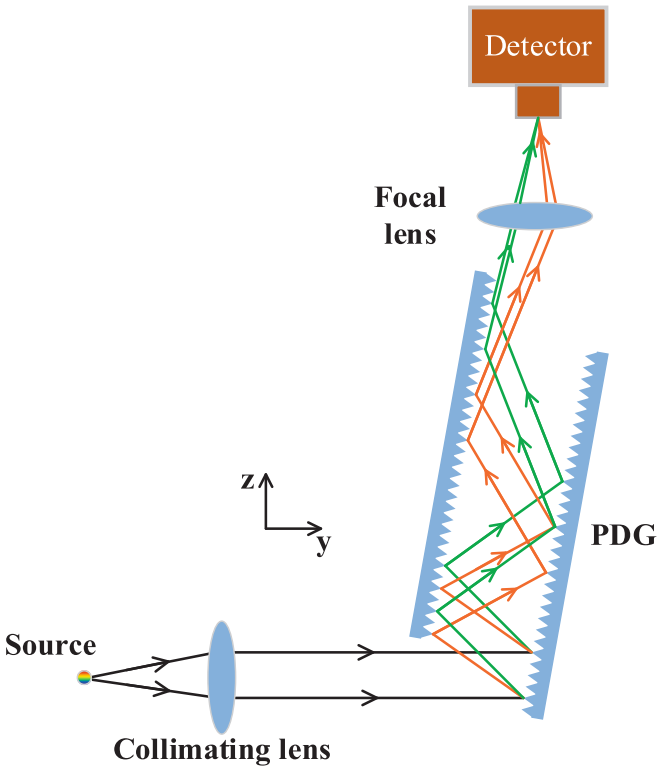

Fig. 1. The schematic of the PDGS.

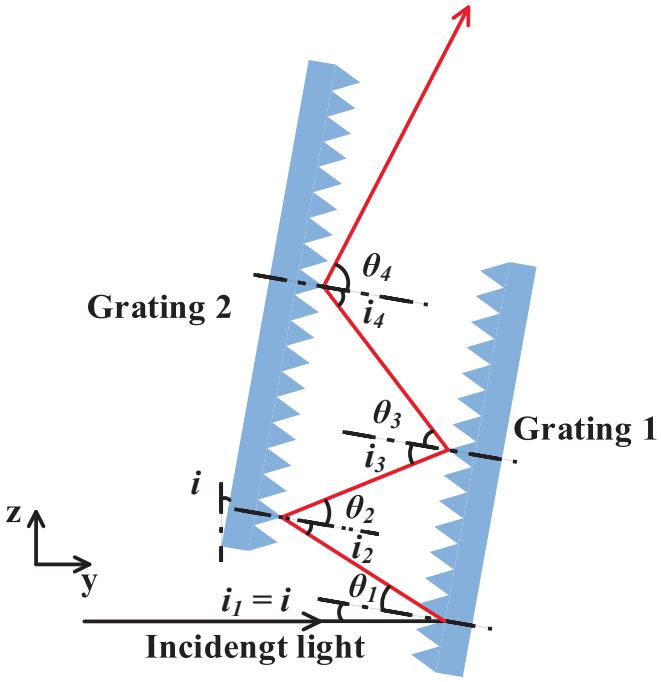

Fig. 2. PDG's light path and theoretical principle.

dispersions, where N could be more than 10, realizing ultra-high spectral resolution. We studied the dispersive principle of the PDG and developed suggestions for appropriate parameter selections for the PDG. After this, detailed numerical simulation analyses were performed to show the characteristics of our design. The conclusions are summarized at the end of this report.

System and principle

The structure of the Parallel-Double-Grating Spectrometer (PDGS) is demonstrated in Fig. 1. The spectrometer has a simple structure, employing lenses as collimating and focusing elements and using gratings as dispersing element. The most distinctive optical device in the proposed spectrometer is PDG, which possesses an uncomplicated structure and provides large angular dispersion. The PDG is composed of two reflective gratings with the same groove density, placed parallel to each other, and the directions of the lines are the same. The signal light is incident on the main section of the grating and diffracted with a specific diffraction order.

A point light source provides the signal light of PDGS. A collimating lens collects the measured light emitted from the point light source and then collimates it. After entering the PDG through the reserved incident area, the measured light repeatedly passes through the two reflective gratings. Because of the diffraction effect, dispersion occurs every time the signal light passes through the grating. In the end, the light will undergo dispersion a total of N times and then leave the PDG. The N-fold dispersed light is focused on the detector with a focusing lens to obtain spectral data.

As shown in Fig. 2, two reflective gratings constituting the PDG are placed in parallel and staggered, leaving enough space so that the measured light can arrive at grating 1 without hindrance. The included angle between the two gratings and z-axis is i. Fig. 2 also depicts the propagation path and angle settings of the measurement light between the two gratings. First, the collimated light reaches grating 1, with the incident angle set to i_1. Due to the geometric relationship of the components, the incident angle i_1 is equal to the inclination angle of the PDG ($i_1 = i$). Then the diffracted signal light leaves grating 1 at the diffraction angle θ_1. Considering the diffracted light to have an order of m, the incident angle i_1 and the diffraction angle θ_1 can be described by the following grating equation:

$$d(\sin i_1 - \sin\theta_1) = m\lambda \tag{1}$$

where d represents the distance between adjacent grooves on the grating surface, λ indicates the wavelength. The incident and diffracted light are on the opposite side of the normal to the grating. The result, $|i_1| < |\theta_1|$, is easily derived from the conditions that $m = -1$. Subsequently, the diffracted light emitted by grating 1 arrives at grating 2 at an incident angle i_2. Because the two gratings are parallel, the incident angle i_2 is equal to the diffraction angle θ_1. By the same reasoning, the diffracted light with an order of -1 with an incident angle of i_2 on grating 2 will exit at a diffraction angle θ_2, satisfying the relationship $|i_2| < |\theta_2|$. The diffracted light emitted from grating 2 will reach grating 1 again, and then grating 2, which means that the incident light will repeat the above process after entering the PDG. After a finite number of diffractions specified as N, the signal light will leave the dispersion component. The PDG has a strong angular dispersion ability arising from the dispersion of the same beam continuously N times.

Angular resolution

An important indicator for evaluating the performance of a spectrometer is angular dispersion, which refers to the angular spacing between two spectral lines within a unit wavelength interval. For a traditional plane reflection grating, the angular dispersion can be calculated according to the grating equation (Eq. (1)):

$$\Gamma = \frac{d\theta}{d\lambda} = \frac{m}{d\cos\theta_1} \tag{2}$$

In the PDG designed in our research, light is diffracted back and forth between two reflective gratings. From a mathematical point of view, this continuous diffraction process is described by repeated iterations of Eq. (1). The diffraction number of beams is N, and the light propagation in

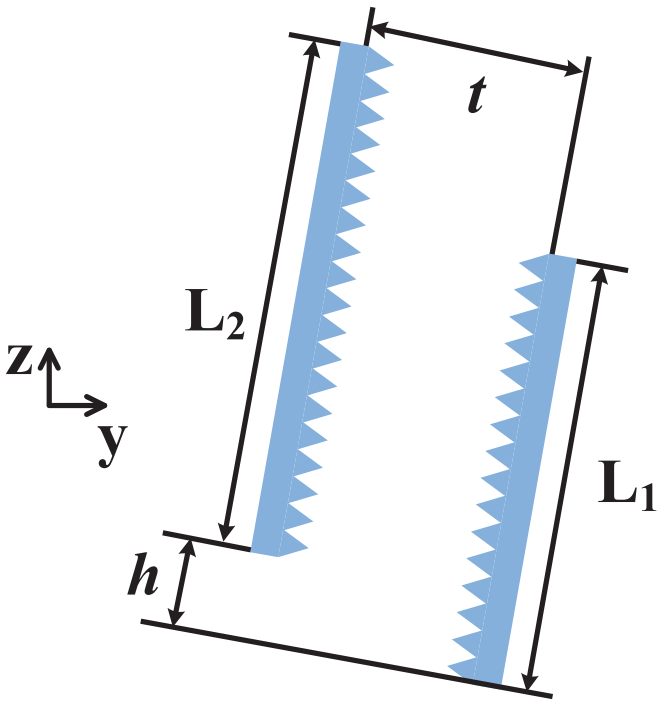

Fig. 3. Structural parameters of the PDG.

the PDG can be described by the following equations:

$$\begin{cases} d(\sin i_1 - \sin\theta_1) = m\lambda \\ d(\sin i_2 - \sin\theta_2) = m\lambda \\ d(\sin i_3 - \sin\theta_3) = m\lambda \\ \vdots \\ d(\sin i_N - \sin\theta_N) = m\lambda \\ i_N = \theta_{N-1} \end{cases} \tag{3}$$

Simplifying Eq. (3), the dispersion equation of the PDG can be obtained as:

$$d(\sin i_1 - \sin\theta_N) = Nm\lambda \tag{4}$$

where i_1 is the initial incident angle, which is determined by the included angle i between the gratings and z-axis, and θ_N is the final diffraction angle of light after diffraction for N times.

Based on the definition of the grating angular dispersion, the expression of PDG's angular dispersion is:

$$\Gamma_N = \frac{d\theta_N}{d\lambda} = \frac{Nm}{d\cos\theta_N} \tag{5}$$

The angular dispersion capability has a positive correlation with the diffraction number N. In addition, the larger the final diffraction angle θ_N, the smaller the cosine value and the stronger the angular dispersion capability of the component. Comparing Eqs. (2) and (5) shows that the angular dispersion capability of the PDG is much larger than that of the plane grating; the ratio Q is:

$$Q = \frac{\Gamma_N}{\Gamma} = \frac{N\cos\theta_1}{\cos\theta_N} \tag{6}$$

Because of $m = -1$, we get the result that $\theta < \theta_N$ which means that compared with the dispersion power of the plane grating, that of the PDG is increased more than N-fold. Such a characteristic significantly improves the angular dispersion power of the grating.

Parameter selection of the PDG

The PDG is composed of two reflective plane diffraction gratings with almost the same parameters. The main parameters of plane grating are its length, width, and groove density. Set the distance between the two gratings as t and the staggering distance as h (the parameter settings are shown in Fig. 3). The grating width is relatively easy to determine because it only needs to be larger than the incident light spot. Before studying the relationship of the grating size parameters, it is necessary to ensure that the incident light can completely enter the PDG, conforming to Eq. (7):

$$t \times \tan(|i_1| + |\theta_1|) \leqslant h \leqslant \frac{t}{\tan|\theta_1|} \tag{7}$$

The value of the grating length L is related to factors such as spot size, diffraction number N, groove density d, incident angle i_1, and grating spacing distance t. If the spot diameter of incident light is D, for grating 1, the grating length L_1 should be determined by:

$$L_1 \geqslant \frac{D}{\cos i_1} + t \times (\tan|\theta_1| + \tan|\theta_2| + \tan|\theta_3| + \cdots + \tan|\theta_{2(x-1)}|) \tag{8}$$

where x is the total number of diffractions by which the incident light is dispersed on grating 1. For grating 2, the grating length L_2 can be calculated by:

$$L_2 \geqslant \frac{D}{\cos i_1} + t \times (\tan|\theta_2| + \tan|\theta_3| + \tan|\theta_4| + \cdots + \tan|\theta_{2(y-1)+1}|) \tag{9}$$

where y is the total number of diffractions by which the incident light is dispersed on grating 2. Furthermore, the two parameters x and y are both positive integers that fulfill the equations $x + y = N$ and $|x - y| \leq 1$. Considering Eq. (4), the relationship between d and θ in Eqs. (8) and (9) is given by:

$$d = \frac{2(x-1)m\lambda}{\sin i_1 - \sin\theta_{2(x-1)}} \tag{10}$$

The spectral resolution

The spectral resolution is an important metric to evaluate the performance of spectrometers, which will be affected by various factors such as the grating dispersion capability, the size of the detector pixel, and the focal length of the imaging lens. To meet the resolution requirements, it is necessary to select the appropriate detector. The resolution capability of the detector can be expressed as:

$$r = \frac{kpd\cos\theta_N}{Nmf} \tag{11}$$

where p is the pixel size, f is the focal length, and k is the number of pixels. The sampling process of the spectral intensity profile should conform to the Nyquist sampling theorem, that is, each spectral point imaged on the detector image surface occupies at least two pixels, so the minimum value of k is 2. Eq. (11) points out that the resolution of the detector is inversely proportional to the pixel size p. Therefore, the smaller the pixel size, the higher the resolution the system can achieve.

Assuming the full width at half maximum of the spectral intensity profile is n pixels, the resolving power R can be calculated using the following equation:

$$R = \frac{\lambda}{\Delta\lambda} = \frac{f(\sin i_1 + \sin\theta_N)}{np\cos\theta_N} \tag{12}$$

where $\Delta\lambda$ refers to the minimum wavelength difference that the dispersive element can distinguish.

Due to Ep. 4, the PDG can be regarded as a special grating with diffraction order Nm. And considering the propagation path of signal light in the PDG, the light passes through the grating N times in total. So, in the ideal case, the equivalent grating line number A can be expressed as:

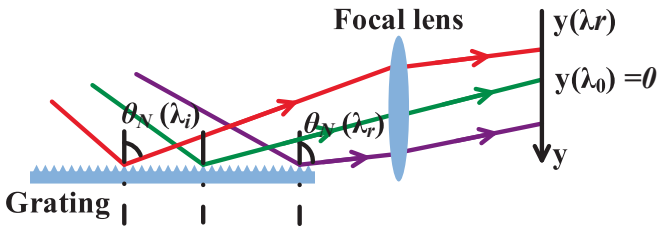

Fig. 4. Diagram of the wavelength calibration principle.

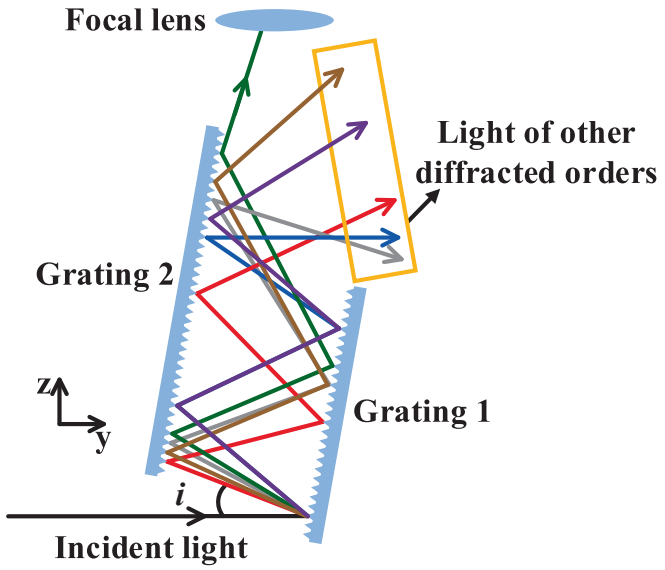

Fig. 5. The propagation process of multi-order diffracted light in PDG.

$$A = \frac{ND}{d\cos i_1} \tag{13}$$

where D/cosi_1 is the projected width of incident light on grating 1. The resolution limit of a grating is the product of the grating line number and the diffraction order. Therefore, the resolution limit of the PDG is:

$$R_{\lim} = \frac{N^2 Dm}{d\cos i_1} \tag{14}$$

Calibration

Because the actual detector has a specific size, which limits the working range of spectrometers, it is necessary to explore the coordinate position distribution of each diffracted beam on the detector. Fig. 4 depicts a schematic diagram of the optical path of the light measured from the PDG through the focusing lens to the detector plane. The signal light with a wavelength of λ_r enters the PDG, leaves at a diffraction angle $\theta_N(\lambda_r)$ after N diffractions, and then converges on the detector plane through the focusing lens. Assuming that $y(\lambda_r)$ is the y-axis coordinate of the light λ_r on the detector, the coordinate of the light λ_i on the y-axis of the detector is specified to be 0, and $\theta_N(\lambda_i)$ is the final diffraction angle of the artificially-set starting wavelength λ_i. Relying on the characteristics of the lenses, geometry, and the law of refraction, the equation to find the y-axis coordinate on the detector plane can be calculated:

$$y(\lambda_r) = f \times \tan(\theta_N(\lambda_r) - \theta_N(\lambda_i)) \tag{15}$$

Combined with Eq. (4), Eq. (13) can be written as:

$$y(\lambda_r) = f \times \tan(\sin^{-1}(\frac{Nm\lambda_r}{d} + \sin i_1) - \sin^{-1}(\frac{Nm\lambda_i}{d} + \sin i_1)) \tag{16}$$

The problem of diffracted light of other orders

The use of low-groove-density gratings inevitably introduces the problem of generating diffracted light of multiple diffraction orders. The problem can be solved by applying blazed gratings. However, the PDG itself is well able to eliminate the influence of multi-order diffracted light. Taking a light with a wavelength of λ as an example, the influence of multi-order beams on PDG is discussed. Basing on Eq. (3), the diffraction orders of light on the PDG are m_1, m_2, m_3 … m_N. The final diffraction exit angle $\theta_{\lambda N}$ of λ can be simplified as follows:

$$\theta_{\lambda N} = \sin^{-1}(\sin i_1 - \frac{M'\lambda}{d}) \tag{17}$$

$$M' = m_1 + m_2 + \cdots + m_N \tag{18}$$

where M' is the sum of the individual diffraction orders. The condition that m_1, m_2, m_3 … m_N are all equal to −1 applies to the propagation mode of the desired light (green light in Fig. 5). The desired exit angle θ_N can be calculated with the following equation due to Eq. (4):

$$\theta_N = \sin^{-1}(\sin i_1 - \frac{Nm\lambda}{d}) \tag{19}$$

We will consider five separate cases for the value of M'.

(1) $M' > 0$. In this case, compared with the desired exit angle θ_N, the final exit angle $\theta_{\lambda N}$ will be much smaller (see Fig. 5 red light). There is even an instance in which the component of the optical propagation vector contains the -z-direction (gray light in Fig. 5).
(2) $M' = 0$. Under this circumstance, the total dispersion of the signal light is 0, and the exit direction is parallel to the incident light (blue light in Fig. 5).
(3) $Nm < M' < 0$. In this instance, the exit angle $\theta_{\lambda N}$ will also decrease (brown light in Fig. 5), but not as much as in case (1). Assuming the propagation distance between focal lens and detector is f, the distance between the light beams with different diffraction orders (M' and Nm respectively) on the detector is P. Taking the light with the diffraction angle θ_N as the reference ray, P can be described as:

$$P = f \times |\tan(\theta_{\lambda N} - \theta_N)| \tag{20}$$

Calculations using the data thus obtained ($i_1 = 6°$, $\lambda = 532$ nm, $M' = -9$, $Nm = -10$, $d = 1/(168$ gr/mm), $f = 150$ mm) reveal that P is about 5.85 cm. When M' decreases, P will be increased. Commonly used detectors are less than 5 cm in length and width and the diffracted light of other orders is unable to arrive upon the detector.

(4) $M' = Nm$, but m_1, m_2 ⋯ m_N are not equal. In the case where $m_2 = -3$, $m_3 = 1$, and the remaining diffraction order is −1. The calculated $\theta_{\lambda N=2}$ is larger than $\theta_{N=2}$ according to diffraction theory. As a result, when the light is subjected to the third diffraction, the distance between the incident point of the two beams is ξ, and remains unchanged until the beams leave the PDG. However, the ξ does not interfere with the results of the detection because the final exit angle does not change.
(5) $M' < Nm$. At this point, $\theta_{\lambda N}$ should be greater than θ_N. However, θ_N is close to 90°, and the diffraction order can only take integer values, which means $M'\lambda$ cannot change continuously, and its value can be only an integer multiple of λ. As a result, $\theta_{\lambda N}$ is greater than 90°, which is impossible in line with diffraction theory. Therefore, the beam cannot diffract N times, and the diffraction order can only be 0 when the light does not meet the diffraction conditions (purple light in Fig. 5). The exit angle $\theta_{\lambda N}$ is equal to the incident angle of the last diffraction, which is very different from θ_N. In summary, the detection result cannot

Table 1
Simulation Parameters.

Parameter	f_1	f_2	d	i	m	t	L_1	L_2	Array size	Pixel size
Value	150 mm	100 mm	168 gr/mm	6°	−1	10 mm	90 mm	70 mm	2048×512	5×5 μm

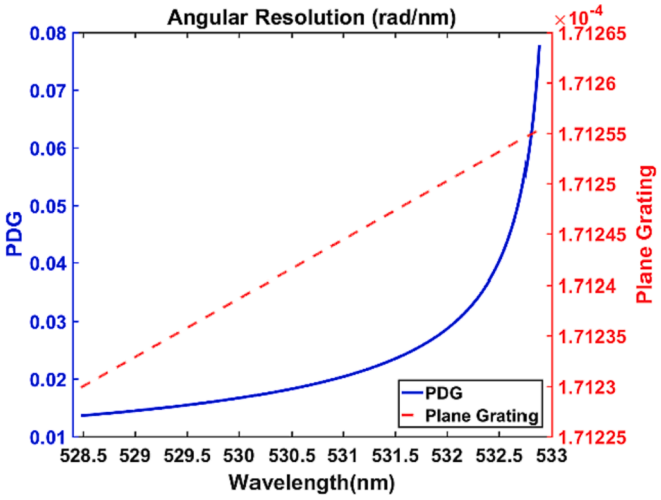

Fig. 6. Comparison of the angular dispersion capability between the PDG and a plane grating.

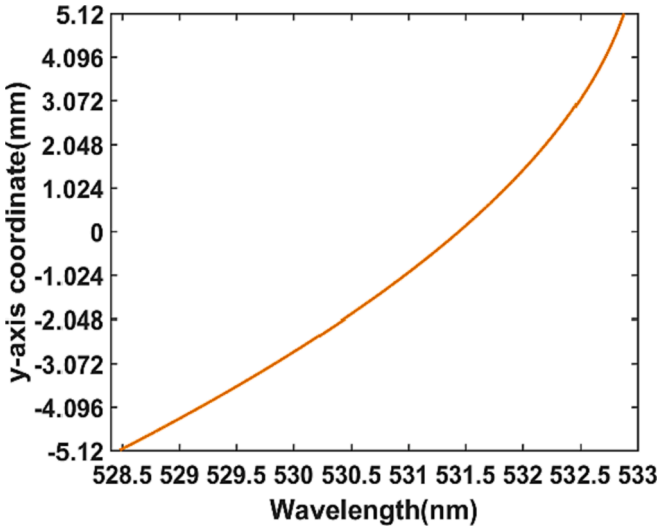

Fig. 7. The y-axis coordinate of different wavelengths on the detector plane.

possibly be affected by the multi-order diffracted light because these rays cannot impinge upon the detector.

Simulation analysis and discussion

Based on the mathematical model above, various parameters of the PDGS were calculated and optimized. The specific structure of the designed spectrometer is illustrated in Fig. 1, and the system parameters used are listed in Table 1. For convenience of discussion, the effect of aberrations is not considered.

In Table 1, f1 represents the focal length of the collimating lens, and f_2 represents the focal length of the imaging lens; d is the grating groove density, where the groove density of the two gratings is the same; i is the incident angle of the signal light, that is, the inclined angle between the PDG and y-axis; m is the diffraction order of the grating; t is the distance between the two gratings; and L_1 and L_2 represent the lengths of grating 1 and grating 2, respectively.

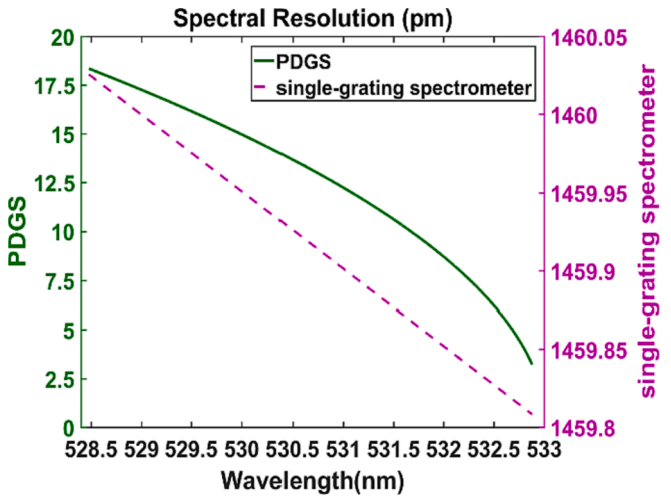

Fig. 8. Comparison of spectral resolution between the PDGS and single grating spectrometer with only one diffraction (theoretical calculation value).

In accordance with the data in Table 1, the calculated angular resolution of the PDG is plotted in Fig. 6 (solid line), and that of a plane grating with the same structural parameters is also shown in Fig. 6 (dotted line). These two curves reveal the substantial difference in the power of angular dispersion between the PDG and the plane grating; the gap increases rapidly as the wavelength increases. At 528.48 nm, the angular dispersion of the PDG and the plane grating are respectively 0.0136 rad/nm and 1.7123×10^{-4} rad/nm, and the ratio of the two reaches 79.6; at 532.88 nm, the angular dispersion of the PDG is the strongest, measuring up to 0.0778 rad/nm. And the ratio reaches 454.3.

From Eq. (16), the y-axis coordinate of different wavelengths on the detector plane is shown in Fig. 7. The angular resolution of the dispersive element is an essential factor affecting the spectral resolution. The larger the angular resolution, the higher the spectral resolution. Therefore, in the long-wavelength band, the distance between the light per unit wavelength difference on the detector plane is greater than that of the short-wavelength wavelength band.

The spectral resolution of the PDGS was calculated, and the results are displayed in Fig. 8. The green solid line denotes the spectral resolution of the spectrometer using PDG, and the magenta dashed line represents the spectral resolution of a single-grating spectrometer with one diffraction. When the incident wavelength is 528.48 nm, the spectral resolution of the PDGS is 18.34 pm; as the wavelength increases, the spectral resolution is improved, just like the angular resolution of the PDG. And at 532.88 nm, the resolution is 3.22 pm. The spectral resolution of the single-diffraction spectrometer is much larger, about 1.46 nm. Compare to the plane grating, a 79.6-fold increase in resolution is easily acquired by employing the PDG.

From the perspective of spectral performance, the detection range of the spectrometer designed in this paper is 528.48–532.88 nm and its spectral resolution is $\leq$18.34 pm. Although the spectrometer has an ultra-high spectral resolution, its bandwidth is 4.4 nm, which limits the scope of applications. However, by rotating the PDG, the measurement bandwidth of the spectrometer can be greatly expanded. When the structural parameters of the PDGS are fixed, the wavelength range that

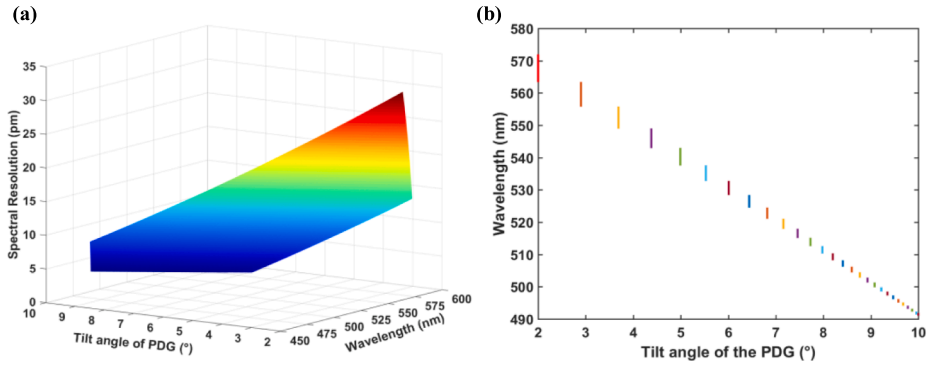

Fig. 9. The effect of rotating the PDG on spectral performance. (a) The influence of tilt angle change on spectral resolution and wavelength range that the PDGS can detect ; (b) Further presentation of the relationship between the dip angle and the measurement band.

Table 2
Theoretical Diffraction Efficiency.

Incident angle of 450 nm (deg)	Efficiency (%)	Incident angle of 530 nm (deg)	Efficiency (%)	Incident angle of 610 nm (deg)	Efficiency (%)
2.0000	88.8422	6.0000	88.0190	10.0000	86.0091
6.3312	91.8890	11.0907	86.4246	15.8210	80.0399
10.6627	84.8127	16.1923	86.9499	21.6927	82.2021
14.9943	81.7464	21.2939	84.5565	27.5643	83.3658
19.3258	79.1148	26.3955	85.5876	33.4360	82.3335
23.6574	79.2473	31.4971	83.0046	39.3077	86.9741
27.9890	75.5316	36.5987	78.9309	45.1793	76.9246
32.3205	66.2367	41.7004	69.7788	51.0510	70.7014
36.6521	59.0649	46.8020	62.5675	56.9227	58.2117
40.9836	51.6150	51.9036	52.2252	62.7944	30.8060
Total	5.4124	Total	7.1506	Total	3.2948

the detector can receive is able to be calculated using Eq. (16). It is obvious that the position where signal beams are imaged at the detector is related to the initial incident angle i_1, which is equal to i, the inclination angle of the PDG. Therefore, the measurement band can be changed by adjusting i. Fig. 9 shows the effect of rotating the PDG on the detection band range and spectral resolution, where Fig. 9(a) illustrates the waveband that the PDGS can detect and its corresponding spectral resolution under different values of i; and Fig. 9(b) further reveals the relationship between dip angle and detection band. It can be found that the value of i plays a vital role in the spectral performance of PDGS. Light in the range of 450 nm to 610 nm can be received by the detector when the angle i changes in a range of 2°-10°, with spectral resolution fluctuating from 2.93 pm to 30.88 pm. When i is equal to 2°, the detectable bandwidth is 8.61 nm; when i increases to 10°, the bandwidth decreases to 0.86 nm, hence they have negative correlations. The relationship between spectral resolution and i is just the opposite, which is a positive correlation. When i is 2°, the lowest and highest resolutions of PDGS are 30.88 pm and 14.64 pm, respectively; when i equals 10°, they are 7.38 pm and 2.93 pm, respectively. The main influence of rotating the PDG is to expand the measurement bandwidth from 4.4 nm to 160 nm.

Then diffraction efficiency is discussed since it affects the signal output intensity of spectrometers. PDGS utilizes multiple diffractions to obtain a high spectral resolution, but this is a trade-off between resolution and diffraction efficiency. To maximize the diffraction efficiency, the PDG consists of two blazed gratings. The energy of the blazed grating is mainly concentrated at a specific diffraction order, and its diffraction efficiency changes slowly with the incidence angle. Taking the blazed grating with a groove density of 168 g/mm and a blazed angle of 9.54° as an example, the efficiency of each diffraction in PDG at 450 nm, 530 nm, and 610 nm is calculated based on Rigorous Coupled Wave Analysis [29]. The initial angle of incidence is 2° for 450 nm, 6° for 530 nm, and 10° for 610 nm. The calculated results are shown in Table 2. After ten diffractions, the total diffraction efficiencies of the PDG for the three selected wavelengths are 5.41 %, 7.15 %, and 3.29 %, respectively, and the average efficiency is about 5.3 %. For those practical applications with relatively relaxed spectral resolution requirements, the value of N can be reduced accordingly to obtain higher output energy. For example, when N is 5, the spectral resolution is lowered by a factor of 1.7 at 530 nm compared to $N = 10$, while the diffraction efficiency is increased by 6.7 times, reaching 47.67 %.

Conclusion

This paper describes a spectrometer using two gratings with a simple parallel structure, which causes the signal light to undergo dispersion N times, realizing pm-level spectral resolution. The number of diffractions N can be customized according to resolution requirements and can be greater than 10. The principle of the spectrometer is analyzed in detail. The research investigates the relationship between performance and structural parameters. The numerical simulation results of a model spectrometer are given, for which the main optical elements called PDG are two plane reflection gratings with the same groove density and different lengths. Compared with the resolution of a single-grating spectrometer, which has the same grating parameters but only one diffraction, that of the PDGS is improved by a factor of 79.6. Changing the tilt angle of the PDG can effectively broaden the measurement bandwidth, enabling detection in a wavelength range of 450–610 nm while maintaining a resolution better than 30.88 pm. The proposed optical path structure is also applicable in the range from ultraviolet to infrared bands by altering the structural parameters appropriately based on the mathematical model. The PDGS has a compact structure, ultra-high resolution, and wide measurement bandwidth, which promises a variety of applications in the field of high-resolution spectral detection.

CRediT authorship contribution statement

Jun Chen: Conceptualization, Methodology, Software, Investigation, Formal analysis, Writing – original draft. **Xiaotian Li:** Conceptualization, Funding acquisition, Resources, Supervision, Writing – review & editing. **Qihang Chu:** Visualization, Investigation. **Jiri Galantu:** Supervision. **Yuqi Sun:** Software, Validation. **Bo Zhang:** Investigation. **Ba Yanheshig:** Resources, Supervision.

Declaration of Competing Interest

The authors declare that they have no known competing financial interests or personal relationships that could have appeared to influence the work reported in this paper.

Data availability

No data was used for the research described in the article.

Funding

This research has been funded by the National Natural Science Foundation of China (Grants 61975255, U2006209, and 61505204), and by Jilin Province Research Projects in China (Grants 20220201083GX).

References

[1] Zeng C, Han Y, Liu B, Sun P, Li X, Chen P. Optical design of a high-resolution spectrometer with a wide field of view. Opt Lasers Eng 2021;140:106547.
[2] O. I. Korablev, J.-L. Bertaux, and I. I. Vinogradov. "Compact high-resolution IR spectrometer for atmospheric studies," in *Infrared Spaceborne Remote Sensing X* (International Society for Optics and Photonics2002). 272-281.
[3] Hachtel JA, Huang J, Popovs I, Jansone-Popova S, Keum JK, Jakowski J, et al. Identification of site-specific isotopic labels by vibrational spectroscopy in the electron microscope. Science 2019;363:525–8.
[4] Ulenikov ON, Gromova OV, Bekhtereva ES, Maul C, Bauerecker S, Gabona M, et al. High resolution ro-vibrational analysis of interacting bands ν4, ν7, ν10, and ν12 of 13C2H4. J Quant Spectrosc Radiat Transf 2015;151:224–38.
[5] Prevedel R, Diz-Muñoz A, Ruocco G, Antonacci G. Brillouin microscopy: an emerging tool for mechanobiology. Nat Methods 2019;16:969–77.
[6] Fiore A, Zhang J, Shao P, Yun SH, Scarcelli G. High-extinction virtually imaged phased array-based Brillouin spectroscopy of turbid biological media. Appl Phys Lett 2016;108:203701.
[7] Pang Y, Zhang Y, Yang H, Huang Z, Jin G. Compact broadband high-resolution infrared spectrometer with a dihedral reflector. Opt Express 2017;25:14960–7.
[8] Aasen H, Bolten A. Multi-temporal high-resolution imaging spectroscopy with hyperspectral 2D imagers–From theory to application. Remote Sens Environ 2018;205:374–89.
[9] Glenn DR, Bucher DB, Lee J, Lukin MD, Park H, Walsworth RL. High-resolution magnetic resonance spectroscopy using a solid-state spin sensor. Nature 2018;555:351–4.
[10] Jerez B, Walla F, Betancur A, Martín-Mateos P, de Dios C, Acedo P. Electro-optic THz dual-comb architecture for high-resolution, absolute spectroscopy. Opt Lett 2019;44:415–8.
[11] Lomsadze B, Cundiff ST. Frequency combs enable rapid and high-resolution multidimensional coherent spectroscopy. Science 2017;357:1389–91.
[12] Richard-Lacroix M, Zhang Y, Dong Z, Deckert V. Mastering high resolution tip-enhanced Raman spectroscopy: towards a shift of perception. Chem Soc Rev 2017;46:3922–44.
[13] Rutkowski L, Masłowski P, Johansson AC, Khodabakhsh A, Foltynowicz A. Optical frequency comb Fourier transform spectroscopy with sub-nominal resolution and precision beyond the Voigt profile. J Quant Spectrosc Radiat Transf 2018;204:63–73.
[14] Sadiek I, Mikkonen T, Vainio M, Toivonen J, Foltynowicz A. Optical frequency comb photoacoustic spectroscopy. PCCP 2018;20:27849–55.
[15] Mhibik O, Forget S, Ott D, Venus G, Divliansky I, Glebov L, et al. An ultra-narrow linewidth solution-processed organic laser. Light Sci Appl 2016;5:e16026–.
[16] Liu Y, Hsu Y, Hsu C-W, Yang L-G, Chow C-W, Yeh C-H, et al. Narrow line-width single-longitudinal-mode fiber laser using silicon-on-insulator based micro-ring-resonator. Laser Phys Lett 2015;13:025102.
[17] Murty M. Theory and Principles of Monochromators, Spectrometers and Spectrographs. Opt Eng 1974;13:23–39.
[18] Wojtkowski M, Srinivasan VJ, Ko TH, Fujimoto JG, Kowalczyk A, Duker JS. Ultrahigh-resolution, high-speed, Fourier domain optical coherence tomography and methods for dispersion compensation. Opt Express 2004;12.
[19] Wang Z, Zhang H, Wang T, Mao B, Meng Y, Li Y, et al. Near-infrared spectrometer based on scanning fiber and linear variable filter. Opt Eng 2021;60:104108.
[20] Reimers J, Bauer A, Thompson KP, Rolland JP. Freeform spectrometer enabling increased compactness. Light Sci Appl 2017;6:e17026–.
[21] Xia G, Wu S, Wang G, Hu M, Xing J. Astigmatism-free Czerny-Turner compact spectrometer with cylindrical mirrors. Appl Opt 2017;56:9069–73.
[22] C. Palmer, and E. G. Loewen. "Diffraction grating handbook." (2005).
[23] Yang Q. First order design of compact, broadband, high spectral resolution ultraviolet-visible imaging spectrometer. Opt Express 2020;28:5587–601.
[24] Lee K-S, Thompson KP, Rolland JP. Broadband astigmatism-corrected Czerny-Turner spectrometer. Opt Express 2010;18:23378–84.
[25] Pang Y, Yao M, Liu S. Grating multiplexing structure based high-resolution infrared spectrometer. Infrared Phys Technol 2020;104:103148.
[26] Yu L, Xue H, Chen J-X. Dual concave grating anastigmatic spectrometer with high spectral resolution for remote sensing. Appl Opt 2018;57:9789–96.
[27] Zhang Y, Wang C, Chen H, Chen S, Guo P, He J, et al. Optical design of a crossed double-grating spectrometer for extracting pure rotational Raman lines of N2. Opt Lasers Eng 2020;134:106291.
[28] Scarcelli G, Yun SH. Multistage VIPA etalons for high-extinction parallel Brillouin spectroscopy. Opt Express 2011;19:10913–22.
[29] Moharam MG, Gaylord TK. Rigorous coupled-wave analysis of planar-grating diffraction. J Opt Soc Am 1981;71:811–8.